HAL
open science

Modeling Urban Impact on Zhengzhou Storm on July 20, 2021

Xiaowen Huang, Dashan Wang, Laurent Z. X. Li, Qi Li, Zhenzhong Zeng

To cite this version:

Xiaowen Huang, Dashan Wang, Laurent Z. X. Li, Qi Li, Zhenzhong Zeng. Modeling Urban Impact on Zhengzhou Storm on July 20, 2021. Journal of Geophysical Research: Atmospheres, 2022, 127, 10.1029/2022JD037387 . insu-03993978

HAL Id: insu-03993978

https://insu.hal.science/insu-03993978

Submitted on 11 Apr 2023

HAL is a multi-disciplinary open access archive for the deposit and dissemination of scientific research documents, whether they are published or not. The documents may come from teaching and research institutions in France or abroad, or from public or private research centers.

L'archive ouverte pluridisciplinaire **HAL**, est destinée au dépôt et à la diffusion de documents scientifiques de niveau recherche, publiés ou non, émanant des établissements d'enseignement et de recherche français ou étrangers, des laboratoires publics ou privés.

Copyright

Check for updates

ADVANCING EARTH AND SPACE SCIENCE

JGR Atmospheres

RESEARCH ARTICLE
10.1029/2022JD037387

Modeling Urban Impact on Zhengzhou Storm on July 20, 2021

Xiaowen Huang[1], Dashan Wang[1], Laurent Z. X. Li[2], Qi Li[3], and Zhenzhong Zeng[1]

[1]School of Environmental Science and Engineering, Southern University of Science and Technology, Shenzhen, China, [2]Laboratoire de Météorologie Dynamique, Centre National de la Recherche Scientifique, Sorbonne Université, Paris, France, [3]School of Civil and Environmental Engineering, Cornell University, Ithaca, NY, USA

Key Points:

- A high-resolution model-based assessment of urban impacts on extreme rainfall for the severe "July-20 event" is presented
- The notable influences of urbanization in shifting the spatiotemporal rainfall patterns and causing storm stagnation are revealed
- Aerodynamic drag effects dominate the differences in the center and south of Zhengzhou during the storm peak

Correspondence to:

D. Wang and Z. Zeng,
wangds6@sustech.edu.cn;
zengzz@sustech.edu.cn

Citation:

Huang, X., Wang, D., Li, L. Z. X., Li, Q., & Zeng, Z. (2022). Modeling urban impact on Zhengzhou storm on July 20, 2021. *Journal of Geophysical Research: Atmospheres*, *127*, e2022JD037387. https://doi.org/10.1029/2022JD037387

Received 25 JUN 2022
Accepted 31 OCT 2022

Author Contributions:

Conceptualization: Dashan Wang, Zhenzhong Zeng
Formal analysis: Xiaowen Huang
Funding acquisition: Dashan Wang, Zhenzhong Zeng
Methodology: Dashan Wang
Resources: Dashan Wang
Software: Dashan Wang
Supervision: Dashan Wang, Zhenzhong Zeng
Visualization: Xiaowen Huang
Writing – original draft: Xiaowen Huang
Writing – review & editing: Dashan Wang, Laurent Z. X. Li, Qi Li, Zhenzhong Zeng

© 2022. American Geophysical Union. All Rights Reserved.

Abstract The heavy storm event that occurred from 18 to 22 July 2021, in Henan province caused severe floods and casualties, especially in the provincial city, Zhengzhou. While the impacts of large-scale synoptic systems and local-scale orographic effects on the storm event have been studied, the role of urbanization remains unexplored. Using Weather Research and Forecasting model, the study designed two numerical experiments, differentiated by the presence of urban land cover, to investigate the urban impact on the storm event over Henan province, with a focus on Zhengzhou. Urbanization increases precipitation in the major urban area of Zhengzhou and its south, western Kaifeng, and western Xuchang, where the largest increases reach from 188.2 to 304.4 mm. Further investigation into Zhengzhou city reveals that urbanization leads to shifted precipitation center and stagnation in the major urban area, resulting in earlier peak rainfall time and more concentrated precipitation. Elevated surface temperature and sensible heat are identified before the peak rainfall arrives, which leads to increased planet boundary layer height, suggesting the contribution of the urban heat island effect. Thermal perturbation and increased surface roughness over urban areas promote vertical uplift and moisture convergence, increasing water vapor and forming storm system drags during the peak precipitation time, thus bringing earlier and higher amounts of precipitation to the major urban area and its south. The study calls for the consideration of the urban effect of extreme storm events and the precaution against waterlogging over urban areas in rapid-developing cities.

1. Introduction

A record-breaking storm took place in Henan province of China from 00 UTC July 18 to 00 UTC 22 July 2021. The storm brought devastating floods and waterlogging to the province, with the precipitation center located in the provincial capital, Zhengzhou. The extreme event caused 292 deaths and 47 people missing in Zhengzhou city, associated with direct economic losses of 53.2 billion yuan (Yin et al., 2022). Zhengzhou meteorological station recorded accumulated rainfall of 817.3 mm during the storm episode, with maximum hourly rainfall of 201.9 mm at 08–09 UTC on July 20, which makes this exceptionally heavy precipitation episode widely known as the "July-20 event" in the scientific community and public media.

Previous studies have revealed the important role of large-scale synoptic systems in this extreme precipitation episode's formation and development (Wei et al., 2022; Xu et al., 2022). The well-established Huanghuai cyclone (situated in southern Henan province first and slowly moved northward to western Henan province) enhanced a low-level jet with the strong southwesterly flow, a crucial circulation for the initiation of the July-20 event. To the south, the two typhoons In-Fa and Cempaka (situated over the Philippine Sea and the South China Sea, respectively) created favorable conditions to transport abundant water vapor from the tropics to the storm area (Ran et al., 2021). In addition to synoptic conditions, local factors also contributed to precipitation intensification. For example, orographic lifting related to Mount Song in the southwest of Zhengzhou and Mount Taihang in the north was identified to make contributions to the heavy precipitation (Ran et al., 2021; Su et al., 2021). Beyond local orographic conditions, it is believed that other factors, such as land use and land cover properties, can also play a role in extreme precipitation event (Pielke Sr et al., 2011). Yet, limited attention has been paid to the potential impacts of local land properties on the record-breaking "July-20 event" (Luo et al., 2022).

Drastic land cover conversion has occurred in China in the past 40 years, and urban area expansion was one of the major types of land conversion (Liu et al., 2020). The most spectacular urban expansion was certainly in the low-lying coastal zone (e.g., agglomerations in the region of Beijing-Tianjin-Hebei, in the Yangtze River Delta, and the Pearl River Delta), but central China including Henan province has experienced accelerating urbanization since 2000 (Liu et al., 2014; Ning et al., 2018). Urban extent is highly relevant to precipitation modification

through land–atmosphere interactions (Han et al., 2014; Shepherd, 2005). Previous studies, both analytical and numerical modeling, revealed a variety of inter-related mechanisms of urban environments that can alter the spatiotemporal features of extreme precipitation, including urban canopy effects, urban heat island effects, and urban aerosol effects (Han & Baik, 2008; Rosenfeld et al., 2008; Thielen et al., 2000). Consequently, urban settings can exert complex impacts on precipitation extremes. For example, they can enhance precipitation by favoring vertical motions, invigorating convective systems, and promoting moisture convergence (Rozoff et al., 2003). Oppositely, they can also reduce precipitation via reduction of convective available potential energy and evapotranspiration decrease (Georgescu et al., 2012; Zhang et al., 2009). Furthermore, the magnitude of urban effects on extreme precipitation can be greatly influenced by diverse synoptic conditions and topographic settings, increasing the uncertainty of changing extreme precipitation characteristics at local scale (Freitag et al., 2018; Wang, Wang, et al., 2021). Urban–atmosphere interactions may display more heterogeneous spatiotemporal variations of extreme precipitation than large-scale systems, and often contribute to extreme events. However, the underlying mechanisms that take responsibility for these events remain uncertain (Qian et al., 2022).

In recent years, the construction of Central Plains urban agglomeration has resulted in explosive urbanization in Henan province (Wang et al., 2020). Located in complex terrain, Henan province has experienced severe extreme precipitation events in the past. For example, a torrential storm lashed Henan province from July 18 to 20 July 2016, with maximum accumulated precipitation of 732 mm recorded, causing 1.67 million people to sufferance (Li et al., 2018). Despite several studies focusing on large metropolitan areas, such as Beijing, Shanghai, and the Pearl River Delta, few studies have investigated the urban impact on extreme precipitation in Henan, including the rapid-growing provincial capital, Zhengzhou, where the center of the urban agglomeration locates. Due to the diverse findings and conclusions in prior studies across different areas, the transferability of the research results from one place to another remains unsettled (Li et al., 2015; Wang J. et al., 2021; Yan et al., 2020), confining the application of the conclusions in these metropolitan areas on Henan. As the population continues to densify in urban areas, cities are expected to face higher risks of extreme precipitation events (Kumar, 2021). Therefore, an investigation into the July-20 storm under recent urbanization is necessary and will provide important insights into urban hazard mitigation and future urbanization in this area.

In this study, the urbanization impacts on the severe "July-20 event" are investigated. Using numerical model simulation, we analyzed the urban effect on the spatiotemporal pattern of the storm by setting up different land cover types in contrast experiments. Furthermore, we focus on the urban area of Zhengzhou city, which has experienced extreme rainfall and significant societal losses, to investigate the potential mechanisms for the observed differences caused by urbanization.

2. Materials and Methods

2.1. Coupled Land-Atmosphere Model Configuration

The advanced research version 4.2.2 of the Weather Research and Forecasting (WRF-ARW) model developed by the National Center for Atmospheric Research was adopted to perform the numerical simulations. Being a non-hydrostatic, three-dimensional, and sophisticated mesoscale model, WRF has been widely used in various research, including regional climate research, hurricane research, and land–atmosphere interactions (Bukovsky & Karoly, 2009; Skamarock et al., 2019; Wang, Wu, et al., 2021). Noah Mosaic Land Surface Model (Li et al., 2013) was coupled with the WRF model to provide reasonable subgrid-scale variability and sensitivity in the land-atmosphere interactions (Wang, Wu, et al., 2021). Rooted in the Noah land surface scheme (Chen & Dudhia, 2001), the Noah mosaic considers various land covers in the calculation of fluxes and surface variables within each grid, which is different from the Noah scheme that only takes the dominant land cover into account. For experiments with urban land cover, the Single-Layer Urban Canopy Model was coupled for better simulation of thermodynamic characteristics and interactions between urban surface and atmosphere (Chen et al., 2011).

Three one-way nested domains were configured, with a grid spacing of 25 km, 5 km, and 1 km, respectively. The horizontal grids were 95×89 for the outermost domain (D01), 150×150 for the middle (D02), and 220×220 for the innermost domain (D03). The outermost domain covered most of eastern China (Figure 1a). The innermost domain was located in the center of Henan province, covering most of the large cities of Henan province, for example, Zhengzhou, Luoyang, and Kaifeng (Figure 1b). The model contained 35 vertical levels, with the upper boundary to be 50 hPa. The initial and boundary conditions were provided by the fifth-generation reanalysis data

21698996, 2022, 22, Downloaded from https://agupubs.onlinelibrary.wiley.com/doi/10.1029/2022JD037387 by Portail BibCNRS INSU, Wiley Online Library on [11/04/2023]. See the Terms and Conditions (https://onlinelibrary.wiley.com/terms-and-conditions) on Wiley Online Library for rules of use; OA articles are governed by the applicable Creative Commons License

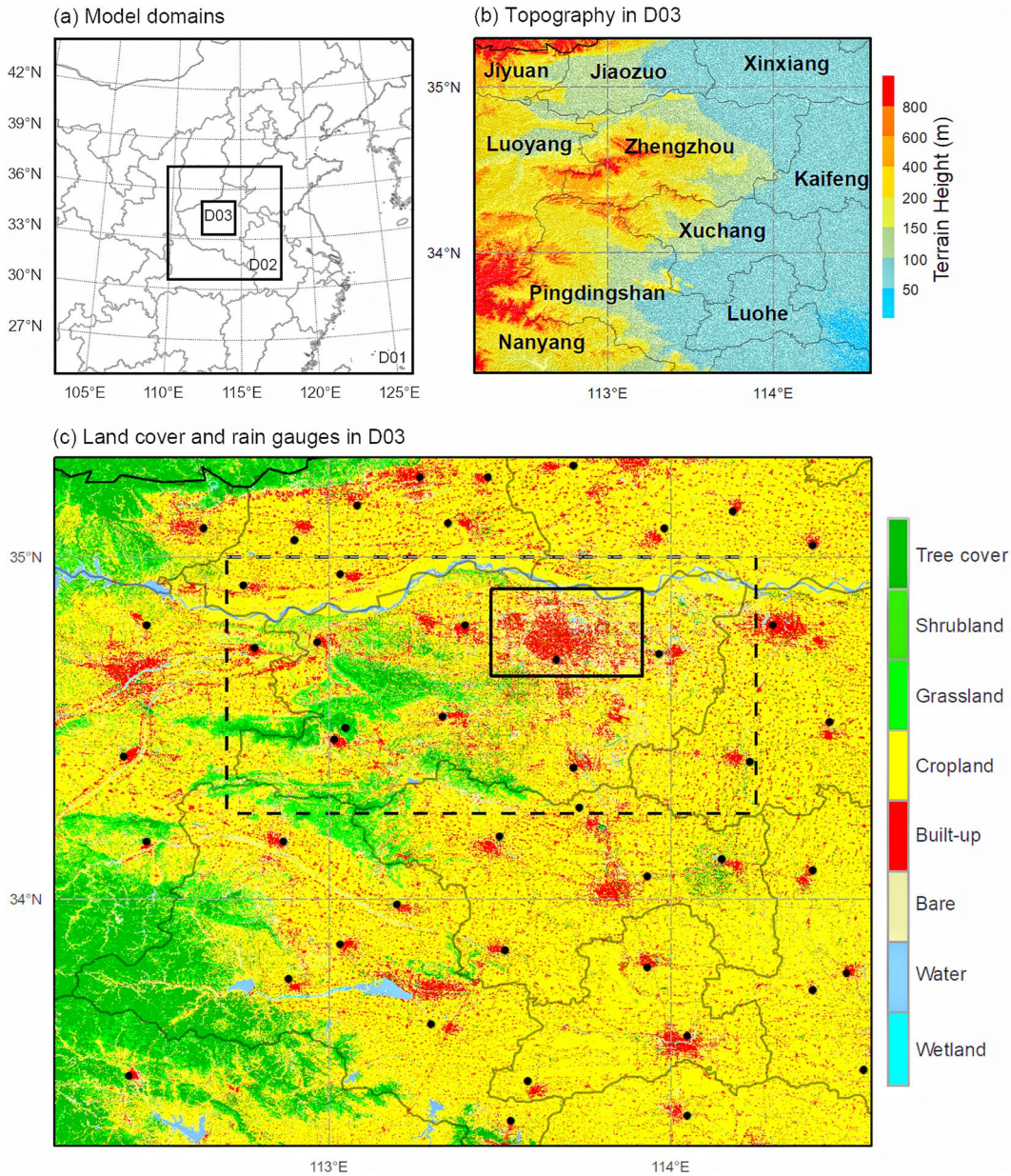

Figure 1. Study region, surface properties, and model domains. (a) Boundaries of the three one-way nested domains D01, D02, and D03; (b) Topography and major cities in domain 3; (c) The spatial pattern of land cover/land use types and the location of meteorological stations (black dots) in domain 3. The large rectangle (dashed line) outlines Zhengzhou city and the small rectangle (solid line) outlines the major urban area (MUA).

(ERA5) of the European Center for Medium-Range Weather Forecasts (ECMWF) with a spatial resolution of 0.25° and a temporal resolution of 1 hr (Hersbach & Dee, 2016).

All simulations shared identical physical schemes (summarized in Table 1). The WRF Single-Moment 6-class scheme was chosen in microphysics as it is recommended for high-resolution simulations (Hong & Lim, 2006). The Rapid Radiative Transfer Model was applied in longwave radiation due to its efficient and accurate fluxes and heating calculation with the correlated-*k* approach (Mlawer et al., 1997). Shortwave radiation used the Dudhia scheme which takes terrain slope and shadow effect on surface solar flux into consideration (Dudhia, 1989). The Yonsei University scheme was employed for planetary boundary layer, as it can parameterize turbulent vertical fluxes of momentum, heat, and constituents, both in the planetary boundary layer and the atmosphere (Hong et al., 2006). The Kain-Fritsch cumulus scheme was adopted for the simulation of convective cloud effects

21698996, 2022, 22, Downloaded from https://agupubs.onlinelibrary.wiley.com/doi/10.1029/2022JD037387 by Portail BibCNRS INSU, Wiley Online Library on [11/04/2023]. See the Terms and Conditions (https://onlinelibrary.wiley.com/terms-and-conditions) on Wiley Online Library for rules of use; OA articles are governed by the applicable Creative Commons License

Table 1
Overview of WRF Physical Schemes

Physics option	Parameterization scheme
Microphysics	WSM 6-class scheme
Longwave radiation	RRTM scheme
Shortwave radiation	Dudhia scheme
Planet boundary layer	Yonsei University scheme
Cumulus	Kain-Fritsch scheme
Land surface	Noah mosaic land surface model
Urban surface	Single-layer UCM
Surface layer	Revised MM5 scheme

(Kain, 2004). Due to the fine grid spacing in D02 and D03 (<10 km), the cumulus scheme was turned off in the two domains (Yang et al., 2021). The surface layer was simulated by the revised MM5 scheme (Jiménez et al., 2012).

2.2. Experimental Design

Two numerical experiments were designed, namely CTRL and NoUrban, differentiated by the presence of urban land cover. As the default land cover in WRF, MODIS 30s land cover product was generated based on the year 2001 (Friedl et al., 2002), the data set could not adequately represent the current land cover under such drastic urbanization in China (Li et al., 2014). Therefore, the "LANDUSEF" and "LU_INDEX" parameters, which were formerly calculated based on default MODIS land cover in the WRF model, were modified according to the WorldCover 2020 v100 product of 10 m resolution released by the European Space Agency (ESA) to more accurately generate the current land use over the study area. The product contains 11 classes of land cover in 2020 and shows an overall accuracy of 74.4%, with the highest accuracy measured in Asia (80.7%; Zanaga et al., 2021). The land cover in D03 included 8 of the 11 classes, namely, tree cover, shrubland, grassland, cropland, built-up, bare/sparse vegetation, permanent water bodies, and herbaceous wetland (Figure 1c). The urban built-up areas are mostly scattered, with the three densest areas located in eastern Luoyang, northeastern Zhengzhou, and western Kaifeng. The 10-m land cover data for 2020 were first aggregated into grids of the same grid spacing in WRF for each domain. The proportion of every class in each 25 km/5 km/1 km grid (f_{ESA}) was calculated. Specifically, the 11 ESA classes were in correspondence with MODIS categories based on one-to-one, one-to-many, or many-to-one relationships (Table 2). For every class with a one-to-one relationship, the modified fraction under MODIS categories ($f_{\mathrm{M_new}}$) was calculated as:

$$f_{\mathrm{M_new}} = f_{\mathrm{ESA}} \tag{1}$$

In one-to-many relationships, $f_{\mathrm{M_new}}$ was calculated based on the original MODIS fraction ($f_{\mathrm{M_ori}}$) and f_{ESA}:

$$f_{\mathrm{M_new},i} = f_{\mathrm{ESA}} \times \frac{f_{M_\mathrm{ori},i}}{\sum_{i=1}^{n} f_{M_\mathrm{ori},i}} \tag{2}$$

where n represented the number of MODIS classes and i ($0 < i \leq n$) denoted the ith MODIS class in each one-to-many relationship. In many-to-one relationships, $f_{\mathrm{M_new}}$ was formulated by:

Table 2
Relationships Between ESA Classification and MODIS 21-Category Land Use Categories

Relationship	ESA category and code	MODIS category and code
One-to-one	**50** Built-up	**13** Urban and Built-up
	70 Snow and Ice	**15** Snow and Ice
	60 Bare/sparse Vegetation	**16** Barren or Sparsely Vegetated
One-to-many	**10** Tree Cover	**1** Evergreen Needleleaf Forest**2** Evergreen Broadleaf Forest**3** Deciduous Needleleaf Forest**4** Deciduous Broadleaf Forest**5** Mixed Forest
	20 Shrubland	**6** Closed Shrublands**7** Open Shrublands
	30 Grassland	**8** Woody Savannas**9** Savannas**10** Grasslands
	40 Cropland	**12** Croplands**14** Cropland/natural vegetation mosaic
	80 Permanent Water Bodies	**17** Water**21** Lake
	100 Moss and Lichen	**18** Wooded Tundra**19** Mixed Tundra**20** Barren Tundra
Many-to-one	**90** Herbaceous Wetland**95** Mangroves	**11** Permanent Wetlands

Note. The bold number denotes the original map code in the classes.

21698996, 2022, 22, Downloaded from https://agupubs.onlinelibrary.wiley.com/doi/10.1029/2022JD037387 by Portail BibCNRS INSU, Wiley Online Library on [11/04/2023]. See the Terms and Conditions (https://onlinelibrary.wiley.com/terms-and-conditions) on Wiley Online Library for rules of use; OA articles are governed by the applicable Creative Commons License

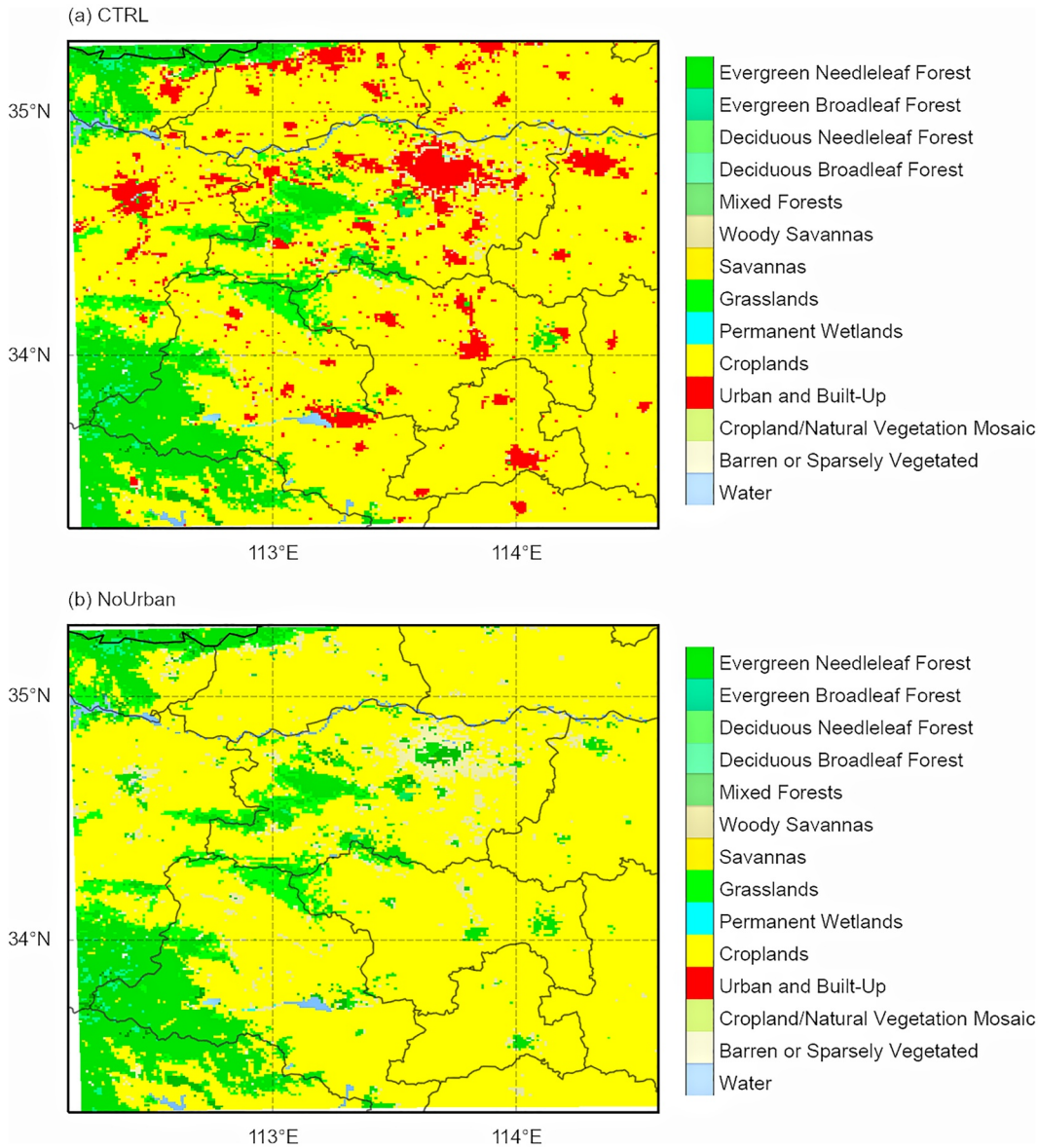

Figure 2. Dominant land category for (a) CTRL and (b) NoUrban simulations in D03.

$$f_{\text{M_new}} = \sum_{j=1}^{m} f_{\text{ESA},j} \tag{3}$$

where m represented the number of ESA classes and j ($0 < j \leq m$) denoted the jth ESA class in each many-to-one relationship. Finally, the "LANDUSEF" and "LU_INDEX" parameters were updated with $f_{\text{M_new}}$ in the CTRL scenario. The NoUrban scenario is the same as CTRL but with modifications in the innermost domain, where the fraction of urban land cover was set to zero, and the fraction of other land cover types except water bodies increased proportionally. Compared with the CTRL scenario, grids that were previously dominated by urban land cover were mostly replaced by forests, croplands, and bare ground in the NoUrban scenario (Figure 2).

The simulation time was set up from 12 UTC on July 18 to 00 UTC on 21 July 2021, which covered the period of the heavy precipitation in Henan (Ran et al., 2021). The output interval was 1 hr for the innermost domain. The first 12 hr were treated as spin-up, which was excluded in the analyses. Observed hourly precipitation data from 47 automatic rain stations in D03 (Figure 1c) provided by the National Meteorological Information Center of the China Meteorological Administration (CMA) was applied to evaluate the model performance of the CTRL

21698996, 2022, 22, Downloaded from https://agupubs.onlinelibrary.wiley.com/doi/10.1029/2022JD037387 by Portail BibCNRS INSU, Wiley Online Library on [11/04/2023]. See the Terms and Conditions (https://onlinelibrary.wiley.com/terms-and-conditions) on Wiley Online Library for rules of use; OA articles are governed by the applicable Creative Commons License

simulation. Correlation coefficient (r) and root-mean-squared-error (RMSE) were used in the evaluation with the common grid-to-point comparison method, and were calculated as follows:

$$r = \frac{\sum_{k=1}^{N}\left(\mathrm{Obs}_k - \overline{\mathrm{Obs}}\right)\left(\mathrm{Sim}_k - \overline{\mathrm{Sim}}\right)}{\sqrt{\sum_{k=1}^{N}\left(\mathrm{Obs}_k - \overline{\mathrm{Obs}}\right)^2}\sqrt{\sum_{k=1}^{N}\left(\mathrm{Sim}_k - \overline{\mathrm{Sim}}\right)^2}} \tag{4}$$

$$\mathrm{RMSE} = \sqrt{\frac{1}{N}\sum_{k=1}^{N}\left(\mathrm{Sim}_k - \mathrm{Obs}_k\right)^2} \tag{5}$$

where Obs_k denoted the k th ($0 < k \leq N$) observational data in overall N data and Sim_k denoted the k th simulated data in the corresponding D03 grid of the k th station.

3. Results

3.1. Model Validation

The CTRL simulation generally captures the spatial pattern in rainfall accumulation and the temporal evolution. The model result matches the observed rainfall pattern in eastern Zhengzhou and other surrounding cities, such as Kaifeng and Xuchang, implying the reasonable performance of WRF in simulating the heavy rainfall episode (Figure 3a). It also successfully simulates the largest rainfall accumulation measured in Zhengzhou station (observed: 732 mm; simulated: 692 mm within 2 days). Although some model grids underestimate the rainfall amount (e.g., grids of Xinmi station, Songshan station, and Gongyi station in western Zhengzhou), the simulation still shows a high spatial correlation with the observation ($r = 0.61$; Figure 3b). In Zhengzhou city, the event's epicenter, the temporal evolution, as depicted over the eight meteorological stations, is well captured over the corresponding model grids, with even a higher agreement if compared to the accumulated rainfall (temporal correlation: $r = 0.79$, RMSE = 5.1 mm). The model captures the rainfall variability during the whole study period, especially the first peak around 04 UTC on July 20, but generally underestimates the overall rainfall intensity and the second peak in 08–09 UTC (Figure 3c). The underestimation at the second peak is likely due to the decreasing simulated rainfall at Zhengzhou station, where the simulation is about half of the observation in 08–09 UTC (Figure 3d). However, the simulated rainfall peak time at Zhengzhou station greatly matches the observed peak time, and the rainfall variation is well captured with $r = 0.72$ and RMSE = 20.6 mm.

3.2. Basic Features of Precipitation Differences Attributed to Urbanization

The NoUrban simulation displays a similar rainfall spatial pattern as in CTRL, but with subtle differences (Figure 4a). The accumulated rainfall also shows a very high amount in Zhengzhou city, with the center shifted westward compared to CTRL. By carefully analyzing the difference between the two simulations, distinct precipitation increases are found near various urban areas, for example, in Zhengzhou's major urban area (MUA) and its south, also in western Kaifeng and western Xuchang (Figure 4b, CTRL-minus-NoUrban showing effects of urbanization). The accumulated precipitation increase can be up to 250.9 mm in the MUA and 304.4 mm in its south, accounting for 55.2% and 91.7% of total precipitation in the 2-day study period in the NoUrban simulation, respectively. In Kaifeng and Xuchang, maximum increments reach 188.2 and 205.3 mm, respectively. The results show strong amplification of rainfall totals near urban areas and suggest important effects of urbanization.

To further confirm the effects of urbanization, we perform statistical analysis, based on the fraction of urban extent of all model grids in the whole area of Zhengzhou city, and in its MUA, respectively (boundaries shown in Figure 1c). Results, stratified into two groups of low and high urban fractions (0–0.2 vs. 0.8–1), are shown in Figure 4c in the form of a probability density function. Model grids with higher urban extent are expected to have larger positive precipitation differences (Figure 4c). Those with low urban fraction (0–0.2) experience mean rainfall differences of −31.5 mm, with smaller variation (standard deviation [STD] = 85.6 mm). The density function shifts positively for grids of high urban fraction (0.8–1), with the mean value increasing to 29.7 mm and the standard deviation to 123.2 mm. The enhancing effect is more pronounced in the MUA of Zhengzhou, where low urban fraction areas have a mean rainfall difference of −72.7 mm and high urban density areas expe-

21698996, 2022, 22, Downloaded from https://agupubs.onlinelibrary.wiley.com/doi/10.1029/2022JD037387 by Portail BibCNRS INSU, Wiley Online Library on [11/04/2023]. See the Terms and Conditions (https://onlinelibrary.wiley.com/terms-and-conditions) on Wiley Online Library for rules of use; OA articles are governed by the applicable Creative Commons License

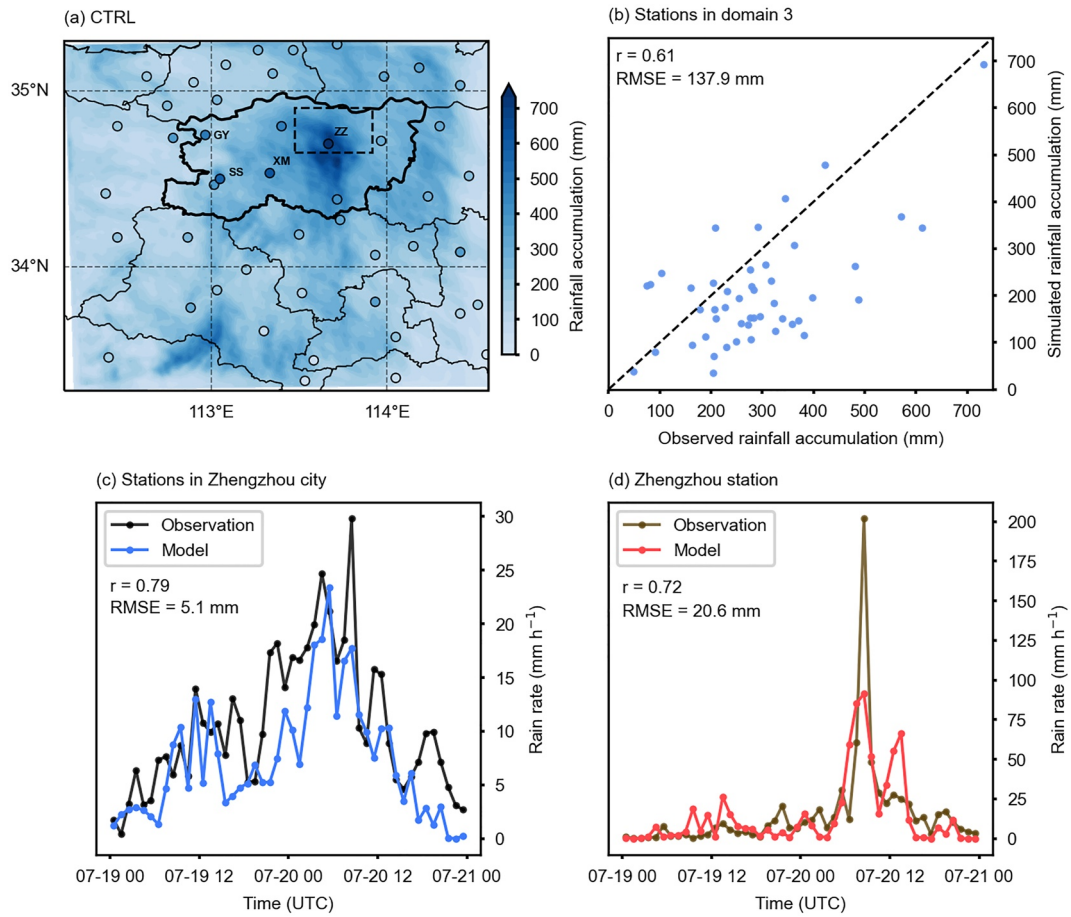

Figure 3. Model validation. (a) Rainfall accumulation of CTRL simulation between 00 UTC 19 July to 00 UTC 21 July, bold line outlines the boundary of Zhengzhou prefectural-level city, "ZZ," "XM," "SS," and "GY" denote Zhengzhou station, Xinmi station, Songshan station, and Gongyi station, respectively; (b) Scatter plots of rainfall amount between stations in domain 3 and the corresponding model grids accumulated from 00 UTC 19 July to 00 UTC 21 July; (c) Time series of hourly rainfall rate (mm hr^{-1}) averaged over the eight stations inside Zhengzhou city (black line) and corresponding model grids (blue line) from the CTRL simulation; (d) Time series of hourly rainfall rate (mm hr^{-1}) of Zhengzhou ("ZZ") station (brown line) and corresponding model grid (red line) from the CTRL simulation.

rience a mean difference of 109.6 mm (Figure 4c). Despite the rainfall amplification near urban areas, negative differences are also detected, especially for the west and the east side of the MUA, where the largest difference surpasses −300 mm (dashed red line in Figure 4c). The negative differences are likely due to the shift of the precipitation center/maxima to the urban areas in the CTRL simulation compared with the NoUrban simulation (Figures 4a and 4b).

The temporal sequences of the CTRL and NoUrban simulations show distinct evolution, as shown in Figure 4d depicting the mean precipitation for the observation obtained over eight meteorological stations and corresponding model grids inside Zhengzhou city. Two peaks are found in the NoUrban simulation, one at 02 UTC on July 20 and another occurring between 09 UTC and 13 UTC on July 20 while in the CTRL scenario, precipitation becomes more concentrated and occurs earlier with one peak during 03–08 UTC on July 20, suggesting urban modification in the temporal evolution of precipitation. The temporal evolution is further investigated through Hovmöller diagrams with precipitation rate averaged over longitude in the domain (Figure 5). The diagrams allow the analysis of the precipitation life cycle as they capture the rainfall propagation in a zonal/meridional direction over time (Goines & Kennedy, 2018). The precipitation zone propagates from east to west before July 20 driven by the southeasterly and easterly flow. Influenced by the Huanghuai cyclone and orographic lifting, then the precipitation zone moves eastward and stagnates in the MUA of Zhengzhou for about 9 hr (from 06 UTC to 15 UTC on July 20), then continue moving eastward (Figure 5a). Meanwhile, another precipitation zone emerges at

21698996, 2022, 22, Downloaded from https://agupubs.onlinelibrary.wiley.com/doi/10.1029/2022JD037387 by Portail BibCNRS INSU, Wiley Online Library on [11/04/2023]. See the Terms and Conditions (https://onlinelibrary.wiley.com/terms-and-conditions) on Wiley Online Library for rules of use; OA articles are governed by the applicable Creative Commons License

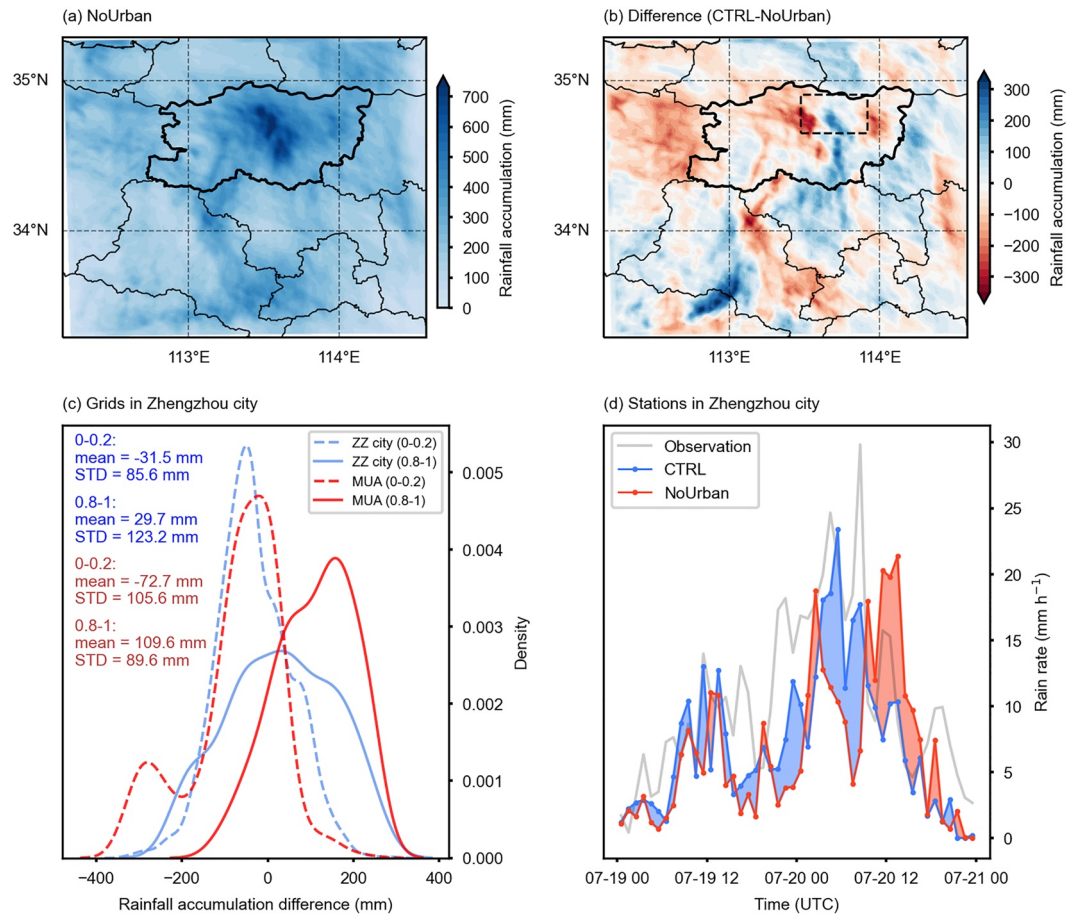

Figure 4. Spatial and temporal patterns. (a) Rainfall accumulation of NoUrban simulation between 00 UTC 19 July to 00 UTC 21 July; (b) Differences in rainfall accumulation between the two simulations (CTRL minus NoUrban). (c) Density curve for rainfall differences of model grids in Zhengzhou city (blue line; dash rectangle outlined in Figure 1c) and major urban area of Zhengzhou (MUA; red line; solid rectangle outlined in Figure 1c) under different urban percentage in model grids (0–0.2: low urban density in dashed line; 0.8–1: high urban density in solid line). (d) Time series of hourly rainfall rate (mm hr^{-1}) averaged over the eight stations inside Zhengzhou city (gray line), and the corresponding model grids from the CTRL simulation (blue line) and NoUrban simulation (red line).

114.5°E around 00 UTC on July 20 and moves westward, then merges with the precipitation in MUA, which may further enhance the precipitation. The stagnation in the CTRL simulation provides high-intensity rainfall over the urban area of Zhengzhou, with the maximum increasing intensity of 19.8 mm hr^{-1}, 4.8 times larger than the intensity in the NoUrban simulation (Figure 5c). The intensified precipitation is mitigated in the NoUrban simulation, where the rain is more evenly distributed, and the peak time is delayed during the same period (Figure 5b).

3.3. Main Drivers for the Urbanization-Induced Precipitation Differences

After the detailed description on the spatiotemporal structures of precipitation changes attributed to urbanization (stagnation of rainfall in the major urban area after a quickly reached peak), we further investigate the precipitation characteristics between 06 UTC and 15 UTC on July 20, which covers the essential part of the heavy precipitation episode (Figure 6, two simulations separately). The precipitation in CTRL is first concentrated in Zhengzhou's MUA and its south (06–09 UTC). One center stagnates in Zhengzhou and another center spreads southward into Xuchang (09–12 UTC) and finally dissipates (12–15 UTC; Figures 6a, 6c, and 6e). In contrast to CTRL, heavy precipitation in NoUrban begins on the west edge of the MUA and then propagates eastward into Kaifeng, passing through the MUA without stagnation (Figures 6b, 6d, and 6f). The different moving speed explains the early peak of precipitation in CTRL. Notably, NoUrban experiences larger rainfall maxima in every 3-hr accumulation (e.g., >300 mm in Figure 6b) than CTRL does. However, due to the rapid propagation of

21698996, 2022, 22, Downloaded from https://agupubs.onlinelibrary.wiley.com/doi/10.1029/2022JD037387 by Portail BibCNRS INSU, Wiley Online Library on [11/04/2023]. See the Terms and Conditions (https://onlinelibrary.wiley.com/terms-and-conditions) on Wiley Online Library for rules of use; OA articles are governed by the applicable Creative Commons License

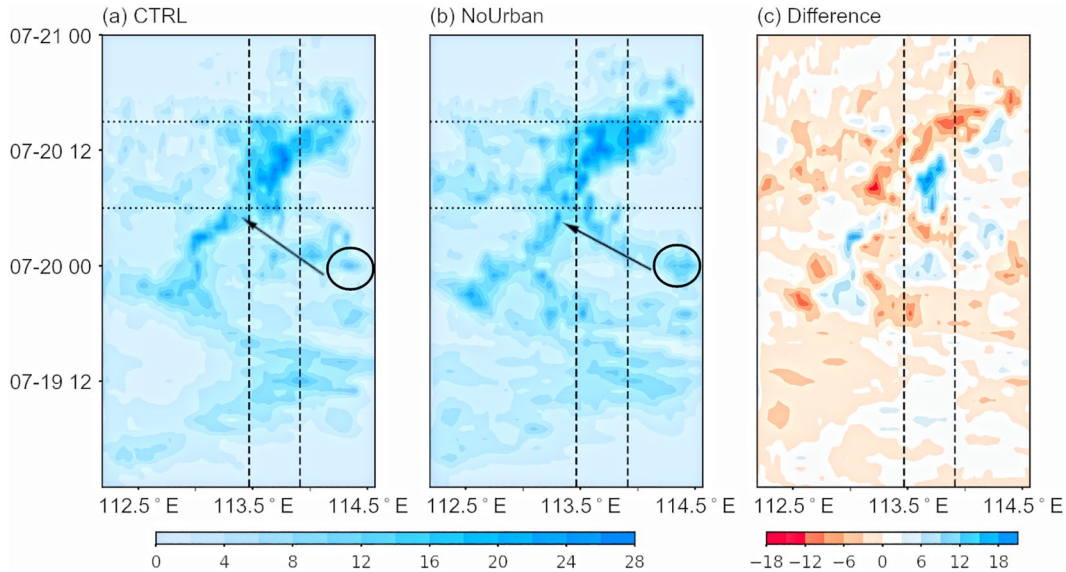

Figure 5. Hovmöller diagrams of hourly rainfall rate (shading, mm hr^{-1}) for (a) CTRL, (b) NoUrban simulations, and (c) their differences from 00 UTC 19 July to 00 UTC 21 July. The rainfall rate is averaged in longitude within domain 3 for each hour. The vertical axis represents time and the horizontal axis represents longitude. Dotted lines denote 06 UTC and 15 UTC on July 20. Dashed lines represent the major urban area of Zhengzhou (shown in Figure 1c). The precipitation zone is circled, and the vector denotes its direction of propagation.

the event, the overall precipitation accumulation is much higher in CTRL for Zhengzhou's MUA. The rapid propagation in NoUrban is also likely the reason to explain the large difference in rainfall rate between the two simulations for the time interval 03–09 UTC (Figure 4d) since those model grids that contain weather stations in Zhengzhou partly miss the rapid-moving system in NoUrban.

Urban impact on precipitation is highly relevant to thermal perturbation, convective activities, and moisture. We observed a slightly increased 2-m temperature associated with enhanced sensible heat flux in the MUA of the Zhengzhou area before the storm peaks around the MUA (Figures 7a and 7b). The higher sensible heat flux likely elevates the planetary boundary layer height, favoring the city's subsequent convective motions at the peak time (Figure 7c). Notably, the two simulations present a rather small difference in maximum convective available potential energy, indicating limited urban impact on atmospheric stability under the strong synoptic background, which may not be the main driver for the urban-induced precipitation difference (Figure 7d).

The drag effects of increasing urban surface roughness seem to be the major contributor to the precipitation anomaly between the two simulations (Figure 7e). Larger friction velocity is observed in the MUA in the CTRL simulation than in the NoUrban simulation before the storm peak, triggering the subsequent effects on local circulation and moisture during the storm peak (Figure 7f). Between 06 and 09 UTC on July 20, enhanced upward motion is found in the MUA of Zhengzhou (Figure 8a). There are two enhanced updrafts, one in the western boundary of the Zhengzhou city (ascending from 850 hPa), and the other appears in the center of MUA, associated with increasing water vapor. The ascending air motion brings a narrow band of moisture upward from the surface, forming enhanced water vapor covering the MUA above 900 hPa, and favoring the heavy rainfall in the MUA due to strong convection (Figure 8a). Meanwhile, decreased water vapor is identified from the ground to 600 hPa in the west of the MUA (06–09 UTC) and later found below 800 hPa in the MUA (09–12 UTC), associated with downward vertical wind (Figure 8b), indicating a more stable lower atmosphere in the city. The downdraft and reduced water vapor content help to explain the negative rainfall difference along the western boundary of the MUA (Figure 4b). During 12–15 UTC, the urban surface continues to promote updraft from the near-surface at the eastern boundary of MUA to around 800 hPa in the MUA center (Figure 8c), in correspondence with the continuous rainfall in the MUA. Increasing water vapor concentrates on the top of the major urban area and its west, suggesting abundant moisture is transported to the MUA. The increased water vapor over urban is also associated with enhanced moisture convergence (Figure 9). During the peak rainfall period (06–15 UTC 20 July),

21698996, 2022, 22, Downloaded from https://agupubs.onlinelibrary.wiley.com/doi/10.1029/2022JD037387 by Portail BibCNRS INSU, Wiley Online Library on [11/04/2023]. See the Terms and Conditions (https://onlinelibrary.wiley.com/terms-and-conditions) on Wiley Online Library for rules of use; OA articles are governed by the applicable Creative Commons License

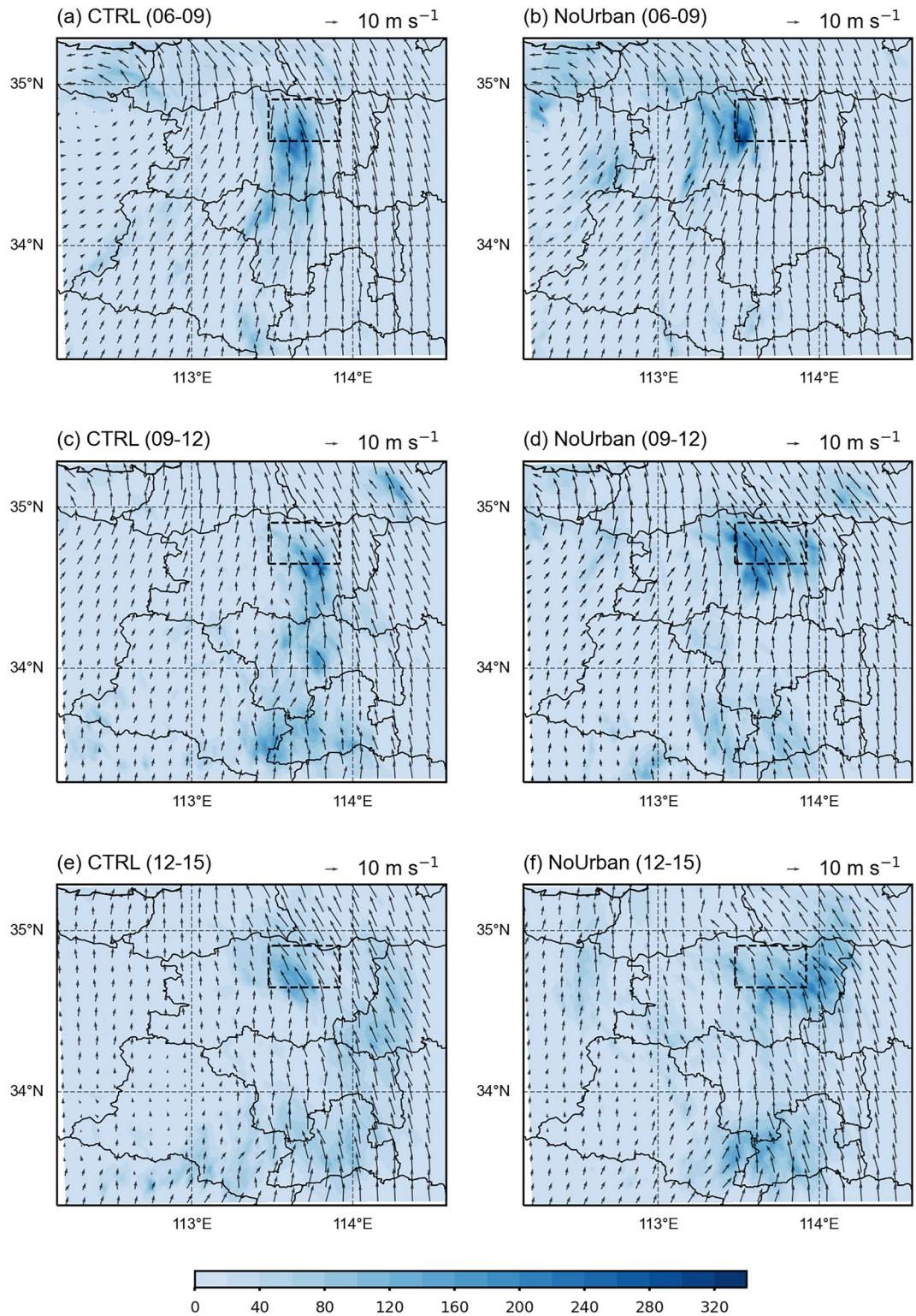

Figure 6. Rainfall accumulation for CTRL and NoUrban simulations in (a–b) 06 UTC-09 UTC 20 July, (c–d) 09 UTC-12 UTC 20 July, and (e–f) 12 UTC-15 UTC 20 July. Vectors denote wind field at 700 hPa. Dashed lines represent the major urban area of Zhengzhou (shown in Figure 1c).

21698996, 2022, 22, Downloaded from https://agupubs.onlinelibrary.wiley.com/doi/10.1029/2022JD037387 by Portail BibCNRS INSU, Wiley Online Library on [11/04/2023]. See the Terms and Conditions (https://onlinelibrary.wiley.com/terms-and-conditions) on Wiley Online Library for rules of use; OA articles are governed by the applicable Creative Commons License

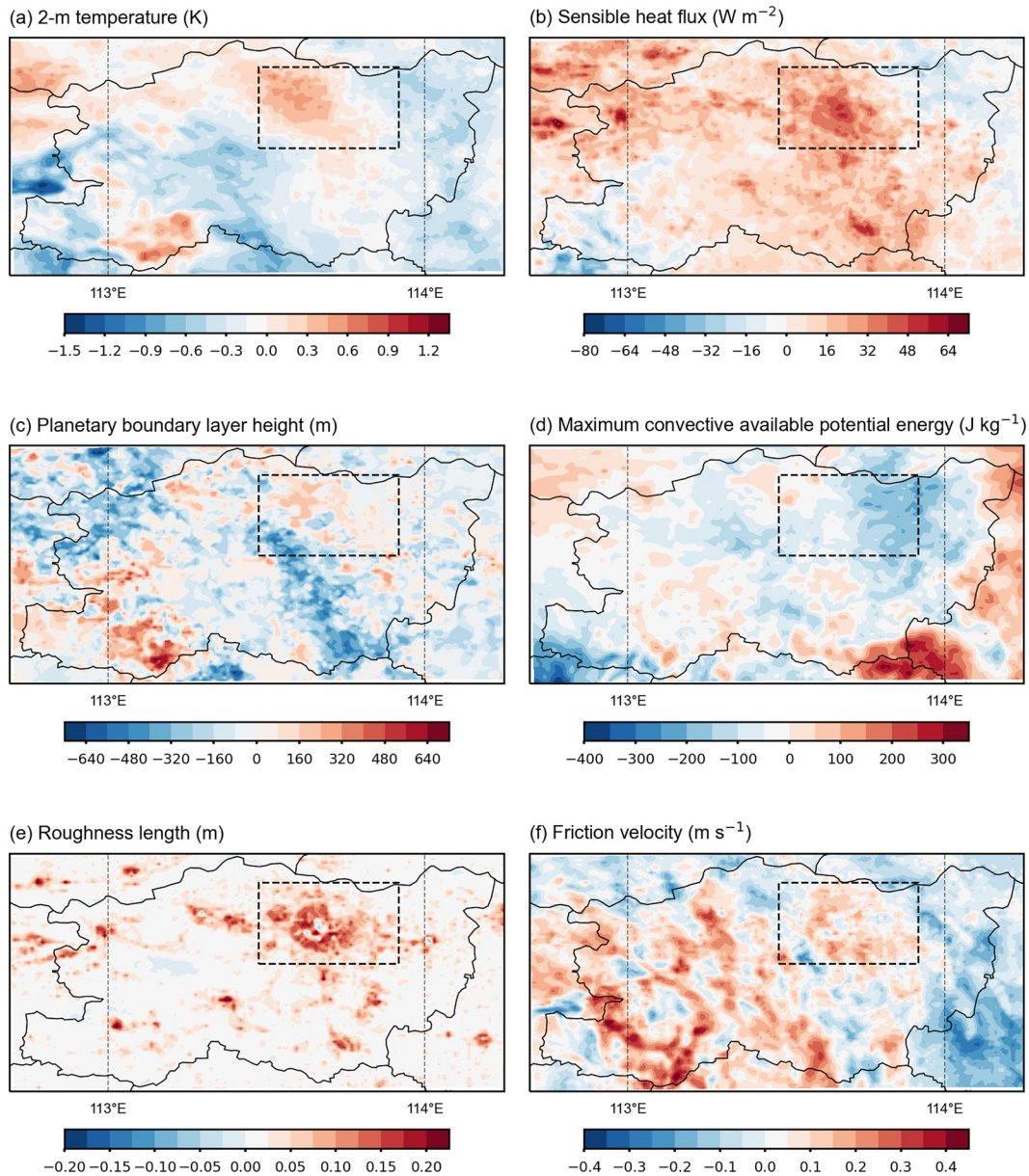

Figure 7. CTRL-minus-NoUrban differences of (a) 2-m temperature, (b) sensible heat flux, (c) planetary boundary layer height, (d) maximum convective available potential energy, (e) roughness length, and (f) friction velocity between 02 and 06 UTC of 20 July in Zhengzhou. Dashed lines represent the major urban area of Zhengzhou (shown in Figure 1c).

enhanced moisture convergence can be identified from the southern boundary of the MUA to the south of Zhengzhou city, explaining the continuously concentrated water vapor and the associated precipitation over these areas.

4. Discussion

The contrast between the two numerical simulations shows that urbanization led to shifted precipitation center, bringing earlier and more concentrated rainfall to the major urban area of Zhengzhou and its south in the "July-20" storm, which is consistent with previous studies of storms in Zhengzhou (Dong et al., 2019; Su et al., 2019). Further investigation reveals the possible roles of urban heat islands (thermodynamic) and urban surface roughness (dynamic) in this storm. Observed elevated near-surface temperature and sensible heat before the storm peak increase the planetary boundary layer height, thus potentially promoting vertical motions and moisture

21698996, 2022, 22, Downloaded from https://agupubs.onlinelibrary.wiley.com/doi/10.1029/2022JD037387 by Portail BibCNRS INSU, Wiley Online Library on [11/04/2023]. See the Terms and Conditions (https://onlinelibrary.wiley.com/terms-and-conditions) on Wiley Online Library for rules of use; OA articles are governed by the applicable Creative Commons License

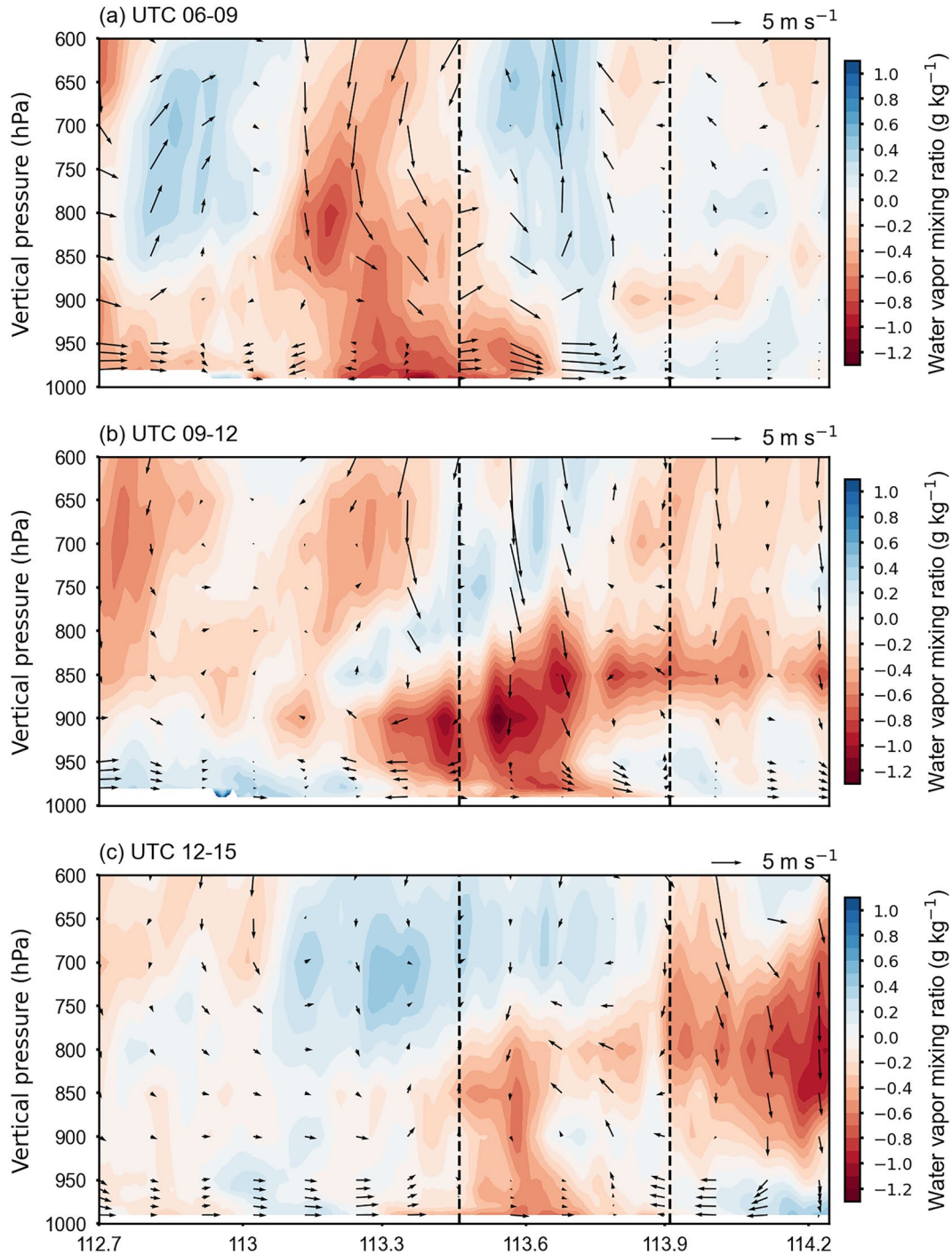

Figure 8. Averaged vertical profiles. 3-hr-averaging vertical profiles of CTRL-minus-NoUrban differences between (a) 06–09 UTC, (b) 09–12 UTC, and (c) 12–15 UTC on 20 July averaged in longitude inside the Zhengzhou city. Shading represents differences in water vapor mixing ratio (g kg^{-1}) and vectors denote composite horizontal and vertical winds (vertical wind multiplied by 10). Dashed lines represent the major urban area of Zhengzhou (shown in Figure 1c).

convergence in the subsequent storm peak (Niyogi et al., 2011). However, thermal impacts on this storm event are likely of less importance compared with surface roughness impact, as the similar study done by Debbage and Shepherd (2019). Aerodynamic drag due to increased surface roughness appears to be the dominant mechanism for urban influence in our analysis. Increasing friction velocity is responsible for the shifted precipitation center, as identified in our study and other studies (Ganeshan & Murtugudde, 2015; Zhang et al., 2018). Since the

21698996, 2022, 22, Downloaded from https://agupubs.onlinelibrary.wiley.com/doi/10.1029/2022JD037387 by Portail BibCNRS INSU, Wiley Online Library on [11/04/2023]. See the Terms and Conditions (https://onlinelibrary.wiley.com/terms-and-conditions) on Wiley Online Library for rules of use; OA articles are governed by the applicable Creative Commons License

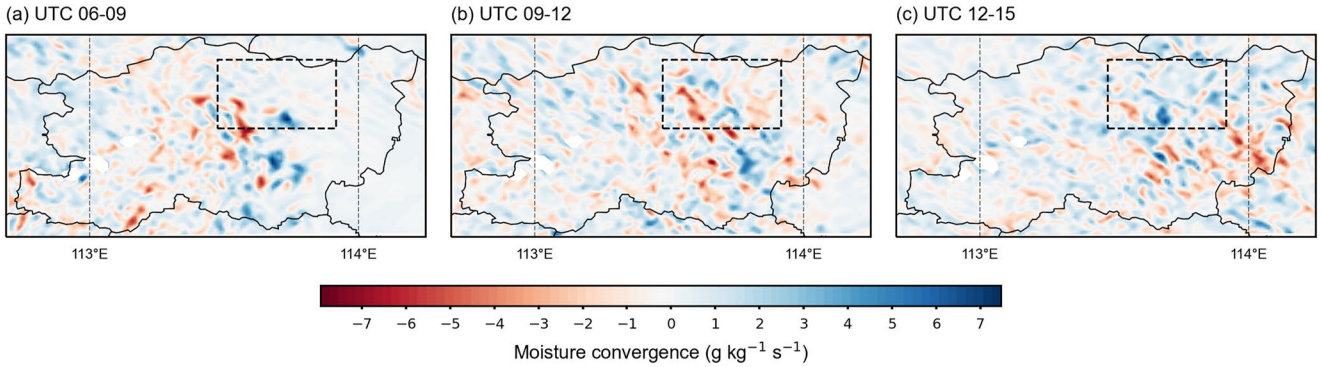

Figure 9. CTRL-minus-NoUrban differences of moisture convergence at 900 hPa (unit: g kg^{-1} s^{-1}) for (a) 06–09 UTC, (b) 09–12 UTC, and (c) 12–15 UTC of 20 July. Positive (negative) values indicate convergence (divergence). Dashed lines represent the major urban area of Zhengzhou (shown in Figure 1c).

MUA is surrounded by scattered urban areas, these areas may provide additional aerodynamic drag to the storm propagation, thereby bringing more precipitation to the MUA and its south (Figure 1c). The aerodynamic drag further affects local circulation by enhancing updrafts and bringing abundant water vapor content to the MUA center, which explains the stagnation over the major urban area of Zhengzhou and the accompanying rainfall increase. Moreover, urban modification in moisture convergence over the regions is identified, which has also been confirmed in other studies (Argüeso et al., 2016; Li et al., 2021). The demonstration of urban surface roughness's impact on moisture transport indicates its effect on storm structure modification and is in agreement with former studies (Li et al., 2021; Shem & Shepherd, 2009; Zhang et al., 2018).

It is noted that our research targets the urban impacts alone, but the extreme event can also be influenced through the combining effects of urbanization and other factors, such as topography. Prior studies have demonstrated the crucial role of topography in precipitation modification (Fairman et al., 2011; Houze, 2012; Navale & Singh, 2020). Cities located in complex terrain may be affected by complex interactions between urban-induced and terrain-induced circulations (Fernando, 2010). Frequent convergence could be produced at the urban interface in urban–orographic interactions (Shepherd, 2006). Freitag et al. (2018) suggested that terrain may amplify urban impacts on weather through persistent forcing of orographic flow. Precipitation amplification by urban-topography interactions may even surpass the effect of topography and urban alone (Yang et al., 2019). Research conducted on heavy precipitation that occurred in Zhengzhou on 5 June 2016, suggested that mountains in the northwest of Zhengzhou could generate gravity waves that promoted convection, leading to increased rainfall in the city (Su et al., 2019). Therefore, for Zhengzhou and its surrounding cities, it can be deduced that the mountains (Mount Song in the west of Zhengzhou, Mount Taihang in the north of Henan province, and the Funiu Mountain in the southwest of Henan province) may play an important role in urban-topography interactions and thus further modify the spatial and temporal patterns of the "July-20" storm event. Understanding urban-orographic interactions in the "July-20" storm still requires additional studies, to be reported in future works.

This research highlights the critical role of the urban land cover effect in the severe storm event on July 20, which may provide insights into future storm analysis and call for precautions against urban waterlogging in Zhengzhou and other fast-growing cities in Henan province. Urban effect in the alteration of storm patterns can bring the precipitation center to the city and promote the stagnation of the storm, therefore increasing the risks of extreme precipitation and flash flood. The results can be further extended to cities worldwide that are rapidly expanding and facing similar synoptic conditions in extreme precipitation events. It is of note that the research may be affected by the lack of consideration of the urban aerosol effect as well as the uncertainties inside the atmospheric models. Additional research and improvement in models can provide further comprehensive and accurate assessments of extreme storm events.

21698996, 2022, 22, Downloaded from https://agupubs.onlinelibrary.wiley.com/doi/10.1029/2022JD037387 by Portail BibCNRS INSU, Wiley Online Library on [11/04/2023]. See the Terms and Conditions (https://onlinelibrary.wiley.com/terms-and-conditions) on Wiley Online Library for rules of use; OA articles are governed by the applicable Creative Commons License

5. Conclusions

The influence of urbanization on modifying the storm event that occurred on 20 July 2021, in Henan province was investigated, with a focus on the provincial city Zhengzhou. Two numerical simulations were designed and run from 12 UTC on July 18 to 00 UTC on July 21, one with the land cover of 2020 and the other replaced urban cover by other land types. Overall, the model accurately depicted the spatial and temporal patterns. Urbanization increased accumulated precipitation in the major urban area of Zhengzhou and its south, western Xuchang, and western Kaifeng. In the provincial city Zhengzhou, urbanization led to shifted precipitation center to the major urban area and rainfall stagnation over and south of the urban area, resulting in earlier peak arrival time and longer storm system stagnation. Increased near-surface temperature and sensible heat in the major urban area were detected before peak precipitation began, suggesting the potential contribution of the urban heat island effect in the storm event. Looking into the peak rainfall time, the effect of urban surface roughness is believed to dominate the differences in the spatiotemporal pattern of the storm. The drag effects due to increased roughness provided pronounced vertical updrafts and increased water vapor content, associated with enhanced moisture convergence in areas with amplified rainfall. The study reveals the need for considering urban effects in storm events for developing cities and can be extended to future extreme storm events with similar synoptic conditions and urban settings, which may provide insights for urban hazard earlier-warning and mitigation.

Conflict of Interest

The authors declare no conflicts of interest relevant to this study.

Data Availability Statement

The WRF-ARW model (Version 4.2.2) is an open-source software with its source code freely available at https://github.com/wrf-model/WRF/releases (Skamarock et al., 2019). ERA5 data (DOI: 10.5065/D6X34W69) used can be retrieved from https://cds.climate.copernicus.eu/cdsapp#!/home (Copernicus Climate Change Services, 2017). The land cover product, ESA Worldcover 2020 is available at https://viewer.esa-worldcover.org/worldcover (Zanaga et al., 2021).The observational precipitation data are provided by the National Meteorological Information Center (NMIC), China Meteorological Administration (CMA), which is confidential and unavailable publicly under national laws. The data can be obtained by applying to the NMIC.

Acknowledgments

This study was supported by the National Natural Science Foundation of China (42071022, 42001321), the start-up fund provided by the Southern University of Science and Technology (29/Y01296122), and the Highlight Project on Water Security and Global Change of the Southern University of Science and Technology (G02296302). We thank the Center for Computational Science and Engineering at the Southern University of Science and Technology for providing computing resources.

References

Argüeso, D., Di Luca, A., & Evans, J. P. (2016). Precipitation over urban areas in the Western Maritime Continent using a convection-permitting model. *Climate Dynamics*, *47*(3), 1143–1159. https://doi.org/10.1007/s00382-015-2893-6

Bukovsky, M. S., & Karoly, D. J. (2009). Precipitation simulations using WRF as a nested regional climate model. *Journal of Applied Meteorology and Climatology*, *48*(10), 2152–2159. https://doi.org/10.1175/2009JAMC2186.1

Chen, F., & Dudhia, J. (2001). Coupling an advanced land surface-hydrology model with the Penn State-NCAR MM5 modeling system. Part I: Model implementation and sensitivity. *Monthly Weather Review*, *129*(4), 569–585. https://doi.org/10.1175/1520-0493(2001)129<0569:CAALSH>2.0.CO;2

Chen, F., Kusaka, H., Bornstein, R., Ching, J., Grimmond, C. S. B., Grossman-Clarke, S., et al. (2011). The integrated WRF/urban modelling system: Development, evaluation, and applications to urban environmental problems. *International Journal of Climatology*, *31*(2), 273–288. https://doi.org/10.1002/joc.2158

Copernicus Climate Change Service. (2017). ERA5: Fifth generation of ECMWF atmospheric reanalyses of the global climate [Dataset]. Copernicus Climate Change Service Climate Data Store. Retrieved from https://doi.org/10.5065/D6X34W69

Debbage, N., & Shepherd, J. M. (2019). Urban influences on the spatiotemporal characteristics of runoff and precipitation during the 2009 Atlanta flood. *Journal of Hydrometeorology*, *20*(1), 3–21. https://doi.org/10.1175/JHM-D-18-0010.1

Dong, J., Liu, C., & Su, A. (2019). Impact of urbanization on a torrential rain process in Zhengzhou region. *Journal of Arid Meteorology*, *37*(6), 922–932. https://doi.org/10.11755/j.issn.1006-7639(2019)-06-0922

Dudhia, J. (1989). Numerical study of convection observed during the winter monsoon experiment using a mesoscale two-dimensional model. *Journal of the Atmospheric Sciences*, *46*(20), 3077–3107. https://doi.org/10.1175/1520-0469(1989)046<3077:NSOCOD>2.0.CO;2

Fairman, J. G., Jr., Nair, U. S., Christopher, S. A., & Mölg, T. (2011). Land use change impacts on regional climate over Kilimanjaro. *Journal of Geophysical Research*, *116*(D3). https://doi.org/10.1029/2010JD014712

Fernando, H. J. S. (2010). Fluid dynamics of urban atmospheres in complex terrain. *Annual Review of Fluid Mechanics*, *42*, 365–389. https://doi.org/10.1146/annurev-fluid-121108-145459

Freitag, B. M., Nair, U. S., & Niyogi, D. (2018). Urban modification of convection and rainfall in complex terrain. *Geophysical Research Letters*, *45*(5), 2507–2515. https://doi.org/10.1002/2017GL076834

Friedl, M. A., McIver, D. K., Hodges, J. C., Zhang, X. Y., Muchoney, D., Strahler, A. H., et al. (2002). Global land cover mapping from MODIS: Algorithms and early results. *Remote Sensing of Environment*, *83*(1–2), 287–302. https://doi.org/10.1016/S0034-4257(02)00078-0

21698996, 2022, 22, Downloaded from https://agupubs.onlinelibrary.wiley.com/doi/10.1029/2022JD037387 by Portail BibCNRS INSU, Wiley Online Library on [11/04/2023]. See the Terms and Conditions (https://onlinelibrary.wiley.com/terms-and-conditions) on Wiley Online Library for rules of use; OA articles are governed by the applicable Creative Commons License

Ganeshan, M., & Murtugudde, R. (2015). Nocturnal propagating thunderstorms may favor urban "hot-spots": A model-based study over Minneapolis. *Urban Climate*, *14*, 606–621. https://doi.org/10.1016/j.uclim.2015.10.005

Georgescu, M., Mahalov, A., & Moustaoui, M. (2012). Seasonal hydroclimatic impacts of Sun Corridor expansion. *Environmental Research Letters*, *7*(3), 034026. https://doi.org/10.1088/1748-9326/7/3/034026

Goines, D. C., & Kennedy, A. D. (2018). Precipitation from a multiyear database of convection-allowing WRF simulations. *Journal of Geophysical Research: Atmospheres*, *123*(5), 2424–2453. https://doi.org/10.1002/2016JD026068

Han, J. Y., & Baik, J. J. (2008). A theoretical and numerical study of urban heat island-induced circulation and convection. *Journal of the Atmospheric Sciences*, *65*(6), 1859–1877. https://doi.org/10.1175/2007JAS2326.1

Han, J. Y., Baik, J. J., & Lee, H. (2014). Urban impacts on precipitation. *Asia-Pacific Journal of Atmospheric Sciences*, *50*(1), 17–30. https://doi.org/10.1007/s13143-014-0016-7

Hersbach, H., & Dee, D. (2016). ERA5 reanalysis is in production. *ECMWF Newsletter*, *147*, 7.

Hong, S.-Y., & Lim, J. (2006). The WRF single-moment 6-class microphysics scheme (WSM6). *Asia-Pacific Journal of Atmospheric Sciences*, *42*, 129–151.

Hong, S.-Y., Noh, Y., & Dudhia, J. (2006). A new vertical diffusion package with an explicit treatment of entrainment processes. *Monthly Weather Review*, *134*(9), 2318–2341. https://doi.org/10.1175/MWR3199.1

Houze, R. A., Jr. (2012). Orographic effects on precipitating clouds. *Reviews of Geophysics*, *50*(1). https://doi.org/10.1029/2011RG000365

Jiménez, P. A., Dudhia, J., González-Rouco, J. F., Navarro, J., Montávez, J. P., & García-Bustamante, E. (2012). A revised scheme for the WRF surface layer formulation. *Monthly Weather Review*, *140*(3), 898–918. https://doi.org/10.1175/MWR-D-11-00056.1

Kain, J. S. (2004). The Kain-Fritsch convective parameterization: An update. *Journal of Applied Meteorology*, *43*(1), 170–181. https://doi.org/10.1175/1520-0450(2004)043<0170:TKCPAU>2.0.CO;2

Kumar, P. (2021). Climate change and cities: Challenges ahead. *Frontiers in Sustainable Cities*, *3*, 5. https://doi.org/10.3389/frsc.2021.645613

Li, D., Bou-Zeid, E., Barlage, M., Chen, F., & Smith, J. A. (2013). Development and evaluation of a mosaic approach in the WRF-Noah framework. *Journal of Geophysical Research: Atmospheres*, *118*, 11918–11935. https://doi.org/10.1002/2013JD020657

Li, H., Wang, X., Zhang, X., Lü, L., & Xu, W. (2018). Analysis on Extremity and characteristics of the 19 July 2016 severe torrential rain in the north of Henan province. *Meteorological Monthly*, *44*(9), 1136–1147. https://doi.org/10.7519/j.issn.1000-0526.2018.09.002

Li, M., Song, Y., Huang, X., Li, J., Mao, Y., Zhu, T., et al. (2014). Improving mesoscale modeling using satellite-derived land surface parameters in the Pearl River Delta region, China. *Journal of Geophysical Research: Atmospheres*, *119*(11), 6325–6346. https://doi.org/10.1002/2014JD021871

Li, Q., Yang, J., & Yang, L. (2021). Impact of urban roughness representation on regional hydrometeorology: An idealized study. *Journal of Geophysical Research: Atmospheres*, *126*(4), e2020JD033812. https://doi.org/10.1029/2020JD033812

Li, Z., Yan, Z., Tu, K., & Wu, H. (2015). Changes of precipitation and extremes and the possible effect of urbanization in the Beijing metropolitan region during 1960-2012 based on homogenized observations. *Advances in Atmospheric Sciences*, *32*(9), 1173–1185. https://doi.org/10.1007/s00376-015-4257-x

Liu, J., Kuang, W., Zhang, Z., Xu, X., Qin, Y., Ning, J., et al. (2014). Spatiotemporal characteristics, patterns, and causes of land-use changes in China since the late 1980s. *Journal of Geographical Sciences*, *24*(2), 195–210. https://doi.org/10.1007/s11442-014-1082-6

Liu, X., Huang, Y., Xu, X., Li, X., Li, X., Ciais, P., et al. (2020). High-spatiotemporal-resolution mapping of global urban change from 1985 to 2015. *Nature Sustainability*, *3*(7), 564–570. https://doi.org/10.1038/s41893-020-0521-x

Luo, Y., Zhang, J., Yu, M., Liang, X., Xia, R., Gao, Y., & Yin, J. (2022). On the influences of urbanization on the extreme rainfall over Zhengzhou on 20 July 2021: A convection-permitting ensemble modeling study. *Advances in Atmospheric Science*. (in press). https://doi.org/10.1007/s00376-022-2048-8

Mlawer, E. J., Taubman, S. J., Brown, P. D., Iacono, M. J., & Clough, S. A. (1997). Radiative transfer for inhomogeneous atmospheres: RRTM, a validated correlated-k model for the longwave. *Journal of Geophysical Research*, *102*(D14), 16663–16682. https://doi.org/10.1029/97JD00237

Navale, A., & Singh, C. (2020). Topographic sensitivity of WRF-simulated rainfall patterns over the North West Himalayan region. *Atmospheric Research*, *242*, 105003. https://doi.org/10.1016/j.atmosres.2020.105003

Ning, J., Liu, J., Kuang, W., Xu, X., Zhang, S., Yan, C., et al. (2018). Spatiotemporal patterns and characteristics of land-use change in China during 2010-2015. *Journal of Geographical Sciences*, *28*(5), 547–562. https://doi.org/10.1007/s11442-018-1490-0

Niyogi, D., Pyle, P., Lei, M., Arya, S. P., Kishtawal, C. M., Shepherd, M., et al. (2011). Urban modification of thunderstorms: An observational storm climatology and model case study for the Indianapolis urban region. *Journal of Applied Meteorology and Climatology*, *50*(5), 1129–1144. https://doi.org/10.1175/2010JAMC1836.1

Pielke Sr, R. A., Pitman, A., Niyogi, D., Mahmood, R., McAlpine, C., Hossain, F., et al. (2011). Land use/land cover changes and climate: Modeling analysis and observational evidence. *Wiley Interdisciplinary Reviews: Climate Change*, *2*(6), 828–850. https://doi.org/10.1002/wcc.144

Qian, Y., Chakraborty, T. C., Li, J., Li, D., He, C., Sarangi, C., et al. (2022). Urbanization impact on regional climate and extreme weather: Current understanding, uncertainties, and future research directions. *Advances in Atmospheric Sciences*, 1–42. https://doi.org/10.1007/s00376-021-1371-9

Ran, L. K., Li, S. W., Zhou, Y. S., Yang, S., Ma, S. P., Zhou, K., & Li, N. (2021). Observational analysis of the dynamic, thermal, and water vapor characteristics of the "7.20" extreme rainstorm event in Henan province, 2021. *Chinese Journal of Atmospheric Sciences*, *45*(6), 1366–1383. https://doi.org/10.3878/j.issn.1006-9895.2109.21160

Rosenfeld, D., Lohmann, U., Raga, G. B., O'Dowd, C. D., Kulmala, M., Fuzzi, S., et al. (2008). Flood or drought: How do aerosols affect precipitation? *Science*, *321*(5894), 1309–1313. https://doi.org/10.1126/science.1160606

Rozoff, C. M., Cotton, W. R., & Adegoke, J. O. (2003). Simulation of St. Louis, Missouri, land use impacts on thunderstorms. *Journal of Applied Meteorology*, *42*(6), 716–738. https://doi.org/10.1175/1520-0450(2003)042<0716:SOSLML>2.0.CO;2

Shem, W., & Shepherd, M. (2009). On the impact of urbanization on summertime thunderstorms in Atlanta: Two numerical model case studies. *Atmospheric Research*, *92*(2), 172–189. https://doi.org/10.1016/j.atmosres.2008.09.013

Shepherd, J. M. (2005). A review of current investigations of urban-induced rainfall and recommendations for the future. *Earth Interactions*, *9*(12), 1–27. https://doi.org/10.1175/EI156.1

Shepherd, J. M. (2006). Evidence of urban-induced precipitation variability in arid climate regimes. *Journal of Arid Environments*, *67*(4), 607–628. https://doi.org/10.1016/j.jaridenv.2006.03.022

Skamarock, W. C., Klemp, J. B., Dudhia, J., Gill, D. O., Liu, Z., Berner, J., et al. (2019). A description of the advanced research WRF Version 4 [Software]. NCAR/TN556+STR, 145. Retrieved from 10.5065/1dfh-6p97

Su, A., Lü, X., Cui, L., Li, Z., Xi, L., & Su, H. (2021). Prediction and test of optimal integrated precipitation based on similar spatial distribution of precipitation. *Torrential Rain and Disasters*, *40*(5), 445–454. https://doi.org/10.3969/j.issn.1004-9045.2021.05.001

21698996, 2022, 22, Downloaded from https://agupubs.onlinelibrary.wiley.com/doi/10.1029/2022JD037387 by Portail BibCNRS INSU, Wiley Online Library on [11/04/2023]. See the Terms and Conditions (https://onlinelibrary.wiley.com/terms-and-conditions) on Wiley Online Library for rules of use; OA articles are governed by the applicable Creative Commons License

Su, A., Shi, D., & Ge, X. (2019). Numerical simulation of the influence from urbanization and orography on a severe rainfall event in Zhengzhou. *Transactions of Atmospheric Sciences*, *42*(3), 434–446. https://doi.org/10.13878/j.cnki.dqkxxb.20181116003

Thielen, J., Wobrock, W., Gadian, A., Mestayer, P. G., & Creutin, J. D. (2000). The possible influence of urban surfaces on rainfall development: A sensitivity study in 2D in the meso-γ-scale. *Atmospheric Research*, *54*(1), 15–39. https://doi.org/10.1016/S0169-8095(00)00041-7

Wang, J., Chen, F., Doan, Q. V., & Xu, Y. (2021). Exploring the effect of urbanization on hourly extreme rainfall over Yangtze River Delta of China. *Urban Climate*, *36*, 100781. https://doi.org/10.1016/j.uclim.2021.100781

Wang, D., Wang, X., Liu, L., Wang, D., & Zeng, Z. (2021). Urban signatures in the spatial clustering of precipitation extremes over mainland China. *Journal of Hydrometeorology*, *22*(3), 639–656. https://doi.org/10.1175/JHM-D-20-0063.1

Wang, D., Wu, J., Huang, M., Li, L. Z., Wang, D., Lin, T., et al. (2021). The critical effect of subgrid-scale scheme on simulating the climate impacts of Deforestation. *Journal of Geophysical Research: Atmospheres*, *126*(17), e2021JD035133. https://doi.org/10.1029/2021JD035133

Wang, J., Hu, C., Ma, B., & Mu, X. (2020). Rapid urbanization impact on the hydrological processes in Zhengzhou, China. *Water*, *12*(7), 1870. https://doi.org/10.3390/w12071870

Wei, P., Xu, X., Xue, M., Zhang, C., Wang, Y., Zhao, K., & Zhu, K. (2022). On the key dynamical processes supporting the 21.7 Zhengzhou record-breaking hourly rainfall in China. *Advances in Atmospheric Sciences*. https://doi.org/10.1007/s00376-022-2061-y

Xu, H., Duan, Y., & Xu, X. (2022). Indirect effects of binary typhoons on an extreme rainfall event in Henan province, China from 19 to 21 July 2021. Part I: Ensemble-based analysis. *Journal of Geophysical Research: Atmospheres*, e2021JD036265. https://doi.org/10.1029/2021JD036265

Yan, M., Chan, J. C., & Zhao, K. (2020). Impacts of urbanization on the precipitation characteristics in Guangdong Province, China. *Advances in Atmospheric Sciences*, *37*(7), 696–706. https://doi.org/10.1007/s00376-020-9218-3

Yang, L., Ni, G., Tian, F., & Niyogi, D. (2021). Urbanization exacerbated rainfall over European suburbs under a warming climate. *Geophysical Research Letters*, *48*, e2021GL095987. https://doi.org/10.1029/2021GL095987

Yang, L., Smith, J., & Niyogi, D. (2019). Urban impacts on extreme monsoon rainfall and flooding in complex terrain. *Geophysical Research Letters*, *46*(11), 5918–5927. https://doi.org/10.1029/2019GL083363

Yin, J., Gu, H., Liang, X., Yu, M., Sun, J., Xie, Y., et al. (2022). A possible dynamic mechanism for rapid production of the extreme hourly rainfall in Zhengzhou city on 20 July 2021. *Journal of Meteorological Research*, *36*(1), 6–25. https://doi.org/10.1007/s13351-022-1166-7

Zanaga, D., VanDe Kerchove, R., De Keersmaecker, W., Souverijns, N., Brockmann, C., Quast, R., et al. (2021). ESA WorldCover 10 m 2020 v100 [Dataset]. Zenodo. Retrieved from 10.5281/zenodo.5571936

Zhang, C. L., Chen, F., Miao, S. G., Li, Q. C., Xia, X. A., & Xuan, C. Y. (2009). Impacts of urban expansion and future green planting on summer precipitation in the Beijing metropolitan area. *Journal of Geophysical Research*, *114*(D2). https://doi.org/10.1029/2008JD010328

Zhang, W., Villarini, G., Vecchi, G. A., & Smith, J. A. (2018). Urbanization exacerbated the rainfall and flooding caused by hurricane Harvey in Houston. *Nature*, *563*(7731), 384–388. https://doi.org/10.1038/s41586-018-0676-z

21698996, 2022, 22, Downloaded from https://agupubs.onlinelibrary.wiley.com/doi/10.1029/2022JD037387 by Portail BibCNRS INSU, Wiley Online Library on [11/04/2023]. See the Terms and Conditions (https://onlinelibrary.wiley.com/terms-and-conditions) on Wiley Online Library for rules of use; OA articles are governed by the applicable Creative Commons License